Full title

Disease-attenuated pneumococcal biosynthesis gene mutants invade the mucosal epithelium and induce innate immunity

Short title

Epithelial microinvasion and innate immunity induction by *Streptococcus pneumoniae*

Caroline M. Weight[1*±], Gabriele Pollara[1], Modupeh Betts[1], Roberta Ragazzini[2], Elisa Ramos-Sevillano[3], Jesús Reiné[4], Matthew Whelan[1], José Afonso Guerra-Assunção[1], Michael Connor[5], Paola Bonfanti[1,2], Clare Jolly[1], Mahdad Noursadeghi[1], Daniela M. Ferreira[4], Jeremy S. Brown[3], Robert S. Heyderman[1±]

[1]Research Department of Infection, Division of Infection and Immunity, UCL London, UK

[2]Francis Crick Institute, London, UK

[3]Department of Respiratory Medicine, UCL, London, UK

[4]Oxford Vaccine Group, University of Oxford, Oxford and Clinical Sciences, Liverpool School of Tropical Medicine, Liverpool, UK

[5]Chromatin and Infection, Institut Pasteur, France

*Current address Biomedical and Life Sciences, Faculty of Health and Medicine, Lancaster University, UK

[±]Corresponding Authors: Dr Caroline M. Weight and Professor Robert S. Heyderman

Email: c.weight@lancaster.ac.uk and r.heyderman@ucl.ac.uk

ABSTRACT

Nasopharyngeal colonisation by *Streptococcus pneumoniae* is characterised by adherence to epithelial cells, microinvasion and innate immune activation. Previously, we have shown that two biosynthesis gene mutants of *S. pneumoniae* serotype 6B strain (Δ*proABC* and Δ*fhs* with an additional Δ*piaA* mutation) can successfully colonise murine and human models without causing disease. Here, we test the hypothesis that epithelial microinvasion and an innate immune response persist despite disease attenuation.

We show that although the Δ*proABC* and Δ*fhs* mutations do not attenuate microinvasion in either experimental human pneumococcal challenge or infection of epithelial cell models, there was less transmigration of Detroit 562 nasopharyngeal epithelial cells by the biosynthesis gene mutants than the WT. Cellular reorganisation by primary human airway epithelial cells varied considerably between strains. Compared to the WT, infection of Detroit 562 epithelial cells by the Δ*fhs/piaA* mutant but not the Δ*proABC/piaA* mutant was less pro-inflammatory, induced less caspase 8 production, associated increased pneumococcal hydrogen peroxide secretion and reduced pneumolysin activity. Under serum stress, these biosynthesis gene mutations had a broad impact on the expression of pneumococcal virulence genes (e.g. *ply*, *nanA* and *psaA*), those regulating oxidative stress (e.g. *SpxB*, *lctO* and *adhE*), and genes involved in purine and carbohydrate metabolism. However, although these may result in disease attenuation, they were not directly linked to effects on microinvasion, cellular reorganisation or the epithelial innate immune response.

These findings suggest that the strain differences observed were driven by the differential expression of multiple bacterial virulence and metabolic pathways, rather than any single gene or pathway of genes. These data highlight the complex impact of single gene mutations on bacterial virulence and suggest that the virulence determinants of pneumococcal epithelial colonisation, microinvasion and innate immunity are not necessarily directly linked to disease.

Author Summary

Streptococcus pneumoniae (the pneumococcus) commonly colonises the back of the human nose, and is a leading cause of pneumonia, meningitis, and sepsis. During colonisation, the pneumococcus adheres to the cells in the nose, invades these cells (so-called microinvasion), and activates them. Colonisation is a pre-requisite for disease, however, since disease is largely a dead end for *S. pneumoniae*, it remains unclear whether these processes are directly linked to disease progression. We have previously shown that if we introduce gene mutations into *S. pneumoniae* that affect key metabolic pathways, these bacteria retain their ability to colonize human and animal models without causing disease. We now show that these mutants retain their ability to microinvade epithelial cells, and some may still cause inflammation, but are less able to pass through the epithelial barrier. However, although the attenuation of disease may be explained by the broad-ranging impact of these mutations on pneumococcal virulence, oxidative stress, and metabolism, they are not driven by a single determinant. Our findings suggest that pneumococcal microinvasion and immune activation are not necessarily pre-cursors to disease progression. This supports the idea that *S. pneumoniae* adapts and evolves to promote colonisation and ultimately transmission rather than cause disease.

Keywords

Biosynthesis genes, host-pathogen interactions, Innate immunity, *Streptococcus pneumoniae*, airway epithelium, colonisation, disease

Graphical Abstract

S. pneumoniae colonisation is characterised by mucus association, epithelial adherence, microcolony formation and microinvasion – where the pneumococcus invades the epithelial barrier without causing disease. Although mutations in *S. pneumoniae* biosynthesis genes (Δ*proABC* and Δ*fhs*) attenuate disease in a murine model, they do not attenuate microinvasion in either experimental human pneumococcal challenge (EHPC) or *in vitro* in primary and immortalised

epithelial cells. Transmigration of the epithelial barrier is attenuated. These mutations show strain-dependent effects on both the epithelial and bacterial responses to infection. Factors such as epithelial cellular reorganisation, inflammation and caspase 8 activity alongside pneumococcal metabolic adaptation, virulence factor expression and response to stress are important components of these processes.

INTRODUCTION

Successful colonisation of the upper respiratory tract (URT) by human pathogens, including bacteria, viruses, and fungi, requires adaptation to the host environment. Pathogens must overcome physical barriers such as mucus, evade antimicrobial peptides, compete with polymicrobial communities, and compensate for nutrient restriction (1). *Streptococcus pneumoniae* (the pneumococcus) is a common commensal of the URT (1), yet translocation of the pneumococcus from the nasopharynx to the lungs, blood or the brain leads to life-threatening disease (1). Among children under five, *S. pneumoniae* is the leading cause of pneumonia-related deaths globally (2).

Using experimental human pneumococcal challenge (EHPC) and epithelial cell models, we have previously shown that colonisation by *S. pneumoniae* is characterised by epithelial surface microcolony formation and invasion of the epithelial barrier without disease, which we have called microinvasion (3). We and others have proposed that pneumococcal colonization elicits an innate immune response that may facilitate clearance while also promoting bacterial transmission (3, 4). The pneumococcal capsule is a key determinant of these processes, influencing epithelial invasion and immune activation (4). Notably, *S. pneumoniae* microinvasion varies between capsular serotypes, with a serotype 4 strain, for example, invading epithelial monolayers more readily and triggering stronger pro-inflammatory responses compared to serotype 6B and 23F strains (3). Beyond the capsule, numerous subcapsular virulence factors and metabolic pathways, such as carbohydrate, nucleotide, fatty acid, and purine/pyrimidine metabolism, further modulate colonization, transmission, and disease potential (5-10). This includes the key virulence determinant pneumolysin, a pore forming pneumococcal toxin which modulates innate immune responses (11, 12). Given the extensive genetic diversity of *S. pneumoniae* (>100 serotypes and >600 global sequence clusters (13)), we contend that pneumococcal virulence has primarily evolved to optimize colonization and transmission rather than to cause invasive disease, which is a dead end. We therefore hypothesize that epithelial microinvasion and the innate immune response triggered during colonization are not necessarily linked to disease causation.

To test this, we have used two *S. pneumoniae* serotype 6B biosynthesis gene mutants (Δ*proABC* and Δ*fhs*), which were designed to induce protective immunity without causing disease (12). These genes, identified through transcriptomic and transposon mutagenesis screens (11,13,14), play critical roles in metabolic adaptation. The *proABC* operon encodes enzymes for proline biosynthesis, while *fhs* encodes a tetrahydrofolate reductase involved in one-carbon metabolism, both essential for pneumococcal growth and virulence (15–17). In murine models, these mutants colonize the nasopharynx comparably to the wild-type (WT) serotype 6B strain (BHN418), but fail to cause invasive disease, despite expressing the same capsule (12,17). In EHPC, where an additional *piaA* deletion (disrupting a key iron uptake transporter) was introduced to prevent reversion to a virulent phenotype (18,19), the Δ*proABC/piaA* and Δ*fhs/piaA* mutants retained the ability to colonise and elicit IgG-mediated immunity (20). These isogenic mutants thus provide a controlled system to investigate epithelial microinvasion and innate immune activation independently of capsular serotype.

Pneumococcal colonisation is a prerequisite for disease. Here, we show that although the Δ*proABC/piaA* and Δ*fhs/piaA* mutations attenuate disease and transmigration of the epithelial barrier, they retain the capacity to colonize and invade epithelial cells in both EHPC and *in vitro* models. Crucially, although this disease attenuation may be explained by the broad-ranging impact of these mutations on pneumococcal virulence, oxidative stress, and metabolism, and despite similar epithelial engagement, we show that that pneumococcal microinvasion and immune activation are not necessarily pre-cursors to disease progression. Together, these findings highlight the complex impact of single gene mutations on pneumococcal virulence, with differential effects on epithelial colonisation and disease.

RESULTS

S. pneumoniae 6B disease-attenuated mutants colonise in EHPC with evidence of epithelial microinvasion

We have defined microinvasion as the process by which *S. pneumoniae* invades the mucosal epithelium without necessarily causing disease (Fig 1A). Nasal curette samples from EHPC healthy volunteers inoculated with the *S. pneumoniae* serotype 6B WT or isogenic mutant strains (Δ*proABC/piaA* or Δ*fhs/piaA*) (14) were collected to investigate the extent of epithelial association and microinvasion. A positive carrier was defined as colonisation at any time point (day 2 or day 6 post-inoculation), as detected by microbiology culture (3). On Day 6 post challenge, carriage was detected by culture in 6/11 volunteers challenged with the WT, 2/11 volunteers with the Δ*proABC/piaA, and* 3/5 volunteers with the Δ*fhs/piaA*. Visualisation of the mucosal cells by confocal microscopy showed colonisation by the WT and mutant pneumococcal strains at day 6 post challenge (Fig 1B): 4/11 volunteers challenged with the WT, 5/11 volunteers with the Δ*proABC/piaA, and* 4/5 volunteers with the Δ*fhs/piaA*. Adherent bacteria were observed in 4/11 volunteers with WT, 3/11 with the Δ*proABC/piaA,* and 4/5 with the Δ*fhs/piaA* strain (Figure 1C). Microinvasion (intracellular bacteria) was seen in 2/11 volunteers with the WT, 5/11 volunteers with the Δ*proABC/piaA,* and 3/5 volunteers with the Δ*fhs/piaA* (Fig 1C). Together, these data show that compared to WT, there was no attenuation of colonisation or microinvasion with either the Δ*proABC/piaA* or Δ*fhs/piaA* strains in EHPC.

S. pneumoniae colonisation and microinvasion of human airway epithelium by the disease-attenuated mutants is associated with cellular reorganisation and preservation of barrier function

We have previously shown that microinvasion by the *S. pneumoniae* 6B WT is characterised by pneumococcal co-association with Junctional Adhesion Molecule A (JAM-A) and β catenin without evidence of barrier dysfunction (3). To further explore whether disease-attenuation influences

epithelial cellular organisation, we cultured *S. pneumoniae* serotype 6B WT and the isogenic biosynthesis mutants with normal human bronchial epithelial airway (NHBE-A) cells in air-liquid interface. We observed epithelial cell association and microinvasion with all three strains (Fig 2A, top). TEM demonstrated that the intracellular bacteria for all three strains were likely enclosed within vacuoles (Fig 2A, bottom). As before, the 6B WT and the mutant strains co-localised with Junctional Adhesion Molecule A (JAM-A, Fig 2B, arrow), with no change in overall JAM-A expression. However, using quantification by image analysis, there were differential effects on the expression of other junctional proteins with an increase in the intensity of Zonula Occludens 1 (ZO-1) at the junctional membrane with the 6B WT strain (Fig 2C, and conversely a significant increase in the intensity of β catenin staining for cells infected (surface or intracellular) with either the Δ*proABC/piaA or* Δ*fhs/piaA* strain (Fig 2D), compared to cells exposed to these strains but were not infected (Fig 2E). These changes in most likely occurred as a result of cellular reorganisation, as de-novo protein production would have been insufficient over the 6-hour experimental infection period. As observed previously (3), epithelial barrier integrity (TEER) was maintained, and indeed increased following infection with the WT and mutant strains (Fig 2F).

We then assessed the possibility that the observed differences in junctional protein organisation between the WT and mutant strains were associated with more wide-ranging effects on epithelial cellular function. When cultured at an air-liquid interface, NHBE cells differentiate into a typical pseudostratified columnar ciliated epithelium, consisting of goblet, Clara, basal and ciliated cells (Fig 3A) but there was no predilection by *S. pneumoniae* for particular epithelial cell-types. Pneumococci were observed amongst cilia (acetylated tubulin positive cells, Fig 3B and Supplemental Information Fig 1) and the Δ*proABC/piaA* strain co-localised with mucus (mucin5ac positive, Fig 3C, arrows). While the cellular composition of the epithelial cultures exposed to the Δ*fhs/piaA* strain were comparable in appearance to non-infected cells by SEM, exposure to the 6B WT and Δ*proABC/piaA* strains resulted in an increased abundance in secreted mucus globules compared to non-infected cells (Fig 3A). This appeared to be due to differential cellular secretion of preformed mucus rather than de-novo production as these differences were not reflected in an increase in the expression of

the gel-forming glycoprotein Mucin5AC (Fig 3C and 3E). Following infection by the Δ*proABC/piaA* strain we found a significant increase in expression of acetylated tubulin within pneumococcal-associated cells (Fig 3B and 3F), which has been shown to be associated with increased microtubule conformation and elasticity, and occurs by post-translational modification (15, 16). In contrast, following exposure to Δ*fhs/piaA* strain but not the other strains, we saw an increased expression of the anti-inflammatory protein, uteroglobin, which is a multifunctional epithelial secreted protein with anti-inflammatory and anti-chemotactic properties, and a marker for non-ciliated Clara cells (Fig 3D and 3G). These changes in uteroglobin expression again most likely occurred as a result of cellular reorganisation, or secretion of pre-formed protein, as de-novo protein production would have been insufficient to detect over the 6-hour experimental infection period. Therefore, although disease attenuation did not appear to influence epithelial colonisation and microinvasion, there were differential effects on epithelial cell organisation which could influence the outcome of colonisation.

Δ*fhs/piaA* but not the Δ*proABC/piaA* mutations attenuate the pro-inflammatory epithelial innate response to pneumococcal colonisation and microinvasion

We have shown that the pattern of Detroit 562 epithelial nasopharyngeal cell microinvasion, and subsequent innate immune response to *S. pneumoniae* 6B infection *in vitro* is similar to that seen in the EPHC *in vivo (3)*. To assess the relationship between disease attenuation and the epithelial innate immune response we have used infection of Detroit 562 epithelial nasopharyngeal cells which enable transcriptomic analysis under multiple conditions, not feasible with sufficient replicates with the primary cell lines. As before, we found that all the strains formed colonies on the epithelial surface (Fig 4A), and although there were small differences, associated comparably with the epithelium (Fig 4B). As seen in the EHPC and the primary epithelial cells, microinvasion of Detroit 562 cells was observed with all the strains (Fig 4C). Differences in microinvasion were not due to differences in intracellular viability (Fig 4D) or replication (Supplemental Information Fig 2A-F). In line with attenuation of disease, the Δ*proABC/piaA* and Δ*fhs/piaA* were impaired in their ability to transmigrate across the epithelium (Fig 4F). Importantly, we also show that a single Δp*iaA* mutation in the *S. pneumoniae* serotype 6B did not affect epithelial association, microinvasion and transmigration (Fig

4B, 4C, 4E). We observed similar effects in Detroit 562 cells compared to airway epithelium for epithelial β catenin expression following incubation with the Δ*proABC/piaA* and Δ*fhs/piaA* strains, compared to the WT in pneumococcal-associated and non-associated cells. (Fig 4F).

Having found that serotype 6B biosynthesis gene mutants that are attenuated for disease retain their capacity for microinvasion in Detroit 562 cells, we have further assessed the link between colonisation, microinvasion and epithelial cell innate immunity by RNAseq. Compared to non-infected cells (Fig 5A), all strains upregulated 78 core epithelial genes related to cytokine signalling in immune system, NLR signalling and GPCR ligand binding. 193 genes were upregulated by both the 6B WT and Δ*proABC/piaA* strains, characterised by Rhodopsin-like receptors, GPCR ligand binding, cytokine signalling in Immune system, signalling by interleukins and Toll Receptor cascades. Infection with the Δ*fhs/piaA* strain resulted in a markedly different transcriptomic profile with modest upregulation of 254 genes, characterised by antigen processing, proteasomal pathways, GTP hydrolysis, and intracellular stress responses (Fig 5A). Overall, the epithelial genes that were most upregulated following infection with 6B WT or Δ*proABC/piaA* strain were similar and contrasted to the reduced gene expression profile seen with the Δ*fhs/piaA* strain despite high levels of cell invasion (Fig 5B). Since both mutant strains contained the *piaA* mutation, this could not account for the differences seen in these responses.

Transcription factors, cellular kinases and cytokines (Fig 5C, 5D) predicted to regulate the differentially expressed genes, showed the greatest difference in profile following infection with Δ*fhs/piaA* strain compared to infection with 6B WT and Δ*proABC/piaA* strains. Δ*fhs/piaA* was predicted to show diminished NFκB and MAPK activation and was associated with a more intrinsic and epithelial repair response that included TBK1, Raf1, JAK1 kinases and IL-1 and IL-33 cytokine signalling. These data therefore suggest that attenuation of disease-causing potential is not dependent on a reduction in the epithelial innate immune response to colonisation.

Enhanced epithelial caspase 8 activity following pneumococcal infection with the wild-type and ∆proABC/piaA strains

To further explore the link between disease attenuation and the epithelial innate immune response to colonisation, we have assessed differential caspase activation. The NLRP3 inflammasome drives programmed epithelial cell death via caspase 1, caspase 3/7 and caspase 8 activity (17). Caspase activity, primarily regulated post-translationally, enables a rapid response to cellular stress and pathogen-mediated activation (18). In health, caspase regulation is thought to be important for mucosal integrity (19). During bacterial pneumonia, caspase activation is thought to have an important pro-inflammatory role, possibly triggered by pneumolysin (20, 21).

Compared to non-infected cells, infection with all strains increased epithelial caspase activity 6-hour post infection, this was significant following infection with ∆*proABC/piaA* strain (Fig 6A, dark grey bars). To test which caspases were activated, we incubated infected cell cultures with either a caspase 1 inhibitor (YVAD-CHO), a caspase 3/7 inhibitor (Z-VAD-FMK), or specifically measured caspase 8 activity. We found that the increase was not due to caspase 1 activity (Fig 6B). Compared to non-infected cells, caspase 3/7 accounted for 3% and 15% of the caspase activity induced following infection with 6B WT and ∆*fhs/piaA* strain respectively (Fig 6A). In contrast, ∆*proABC/piaA* strain did not induce caspase 3/7 activity. Caspase 8 activation was significantly increased following epithelial infection with 6B WT and ∆*proABC/piaA* strain (Fig 6C).

***fhs* gene mutation in *S. pneumoniae* 6B is associated with increased pneumococcal hydrogen peroxide secretion and decreased pneumolysin activity**

S. pneumoniae SpxB and LctO generate hydrogen peroxide (H_2O_2) which has been shown to suppress ENaC-α transcription and inhibit the Na+–K+ pump, acting as an intracellular signal to increase mitochondrial production of ROS (22, 23). We postulated that the differences in cellular

reorganisation, the innate inflammatory response and caspase 8 activation seen between Δ*proABC/piaA* and Δ*fhs/piaA* mutants could be explained by differential expression of pneumococcal H_2O_2. After three and six hours, we detected significantly higher levels of H_2O_2 in Δ*fhs/piaA* cultures compared to 6B WT and Δ*proABC/piaA* strains (Fig 7A). Furthermore, this was maintained during epithelial cell contact (Fig. 7B).

Pneumolysin can both activate and suppress the host innate immune response and mediates the haemolytic activity characteristic of the pneumococcus (12, 24, 25). H_2O_2 increases the release of pneumolysin but paradoxically also negatively impairs its haemolytic activity (26). In line with this paradoxical effect the higher production of H_2O_2 by the Δ*fhs /piaA* strain, was associated with increased *ply* gene expression (see below) but reduced red blood cell lysis compared to 6B WT and Δ*proABC* (Fig. 7C). Differential pneumococcal H_2O_2 release and potential impact on pneumolysin a key virulence factor and pro-inflammatory mediator may therefore explain at least in part, differential the effects of the *S. pneumoniae* serotype 6B Δ*fhs /piaA* but again not the attenuation of disease potential.

Deletion of the *proABC* and *fhs* genes have broad-ranging differential effects on the *S. pneumoniae* virulence gene expression and metabolic gene pathways when under stress

We have previously shown that under serum stress in which optimal nutrient conditions in THY was compared to growth in human serum to represent the physiological stress found during human infection, the Δfhs and ΔproABC mutants showed considerable derangement in global gene transcription (27). Metabolic analysis suggested that Δfhs had an impaired stringent response, and when cultured in sera, both mutants were under increased oxidative stress and had altered lipid profiles (27). The ΔproABC mutation resulted in the accumulation of glycolytic pathway intermediates and peptidoglycan synthesis. To further understand the link between disease attenuation, epithelial colonisation and the innate immune response, we have extended the transcriptomic analysis of the response of the mutants to serum stress (27). This revealed upregulation of well-characterised

pneumococcal virulence factors such as *ply*, *nanA*, *psaA,* those regulating oxidative stress such as *SpxB*, *lctO* and *adhE*, and genes involved in purine and carbohydrate metabolism (Supplemental Information Table 1). Phosphotransferase systems, amino nucleotide sugar, fructose and mannose and metabolic pathways were the most significantly enriched pathways in the Δ*proABC* mutant (Table 1). In contrast, competence, purine, pyruvate, metabolic pathways, amino nucleotide sugar pathways and secondary metabolites were the most significantly enriched pathways in the Δ*fhs* mutant under stress (Table 1). Together these data support or previous contention that deletion of the *proABC* and *fhs* genes have widespread but differential effects on *S. pneumoniae* virulence, metabolism which may account for their disease attenuation and unlinked differential effects on cellular reorganisation and the innate immune response.

Table 1. Differentially expressed pathways from single isogenic mutants in human serum compared to WT.

Pathway	GeneRatio	P-adjust	qvalue
Δ*fhs* vs. WT			
Fatty acid metabolism/biosynthesis	10/57	1.08E-09	6.49E-10
Biosynthesis of secondary metabolites	26/57	2.09E-04	1.26E-04
Purine metabolism	10/57	1.34E-03	8.06E-04
Quorum sensing	11/57	3.20E-03	1.92E-03
Pantothenate and CoA biosynthesis	5/57	3.59E-03	2.16E-03
beta-Lactam resistance	5/57	7.59E-03	4.57E-03
Propanoate metabolism	4/57	1.51E-02	9.09E-03
2-Oxocarboxylic acid metabolism	4/57	1.51E-02	9.09E-03
Metabolic pathways	40/57	1.94E-02	1.16E-02
Amino sugar and nucleotide sugar metabolism	7/57	4.22E-02	2.54E-02

Pyruvate metabolism	5/57	4.31E-02	2.59E-02
Δ*proABC* vs. WT			
Fatty acid metabolism/biosynthesis	10/71	1.17E-08	8.94E-09
Galactose metabolism	12/71	1.25E-04	2.47E-08
Phosphotransferase system (PTS)	13/71	2.54E-03	1.93E-03
Amino sugar and nucleotide sugar metabolism	9/71	2.89E-02	2.20E-02

Table 1. Differentially expressed pathways from single isogenic mutants in human serum compared to WT. 55 genes were selected within competence pathways, amino acid metabolism, virulence factors, oxidative stress pathways and other known genes important for colonisation, for assessment of changes in gene expression following serum stress. *q-value* measures the proportion of false positives incurred (the false discovery rate) when that particular test is significant.

DISCUSSION

There is considerable variation in the ability of different *S. pneumoniae* strains to colonise the human host, cause invasive disease and transmit to others (1). Previously, pneumococcal colonization of the nasopharyngeal niche was thought to be limited to the mucus layer and epithelial surface (1). However, using EHPC, we have shown that pneumococcal microinvasion occurs in healthy volunteers (3). In this study, we show that even when using isogenic serotype 6B biosynthesis pathway mutant strains, attenuated for systemic disease but not for carriage, microinvasion is preserved (27) (28). Notably, epithelial barrier transmigration was significantly less with the isogenic strains with the Δ*fhs/piaA* and Δ*proABC/piaA* mutations compared to WT *S. pneumoniae* 6B. Pneumococcal colonization and microinvasion of primary human airway epithelium were associated with cellular reorganization and while maintaining barrier integrity. However, neither these structural

changes nor the associated inflammatory response correlated with disease attenuation. Under stress conditions, the Δ*proABC* and Δ*fhs* mutations led to upregulation of multiple metabolic pathways, presumably as a compensatory mechanism. Additionally, these mutations increased the expression of several pneumococcal virulence factor genes (Graphical Abstract Summary), which may explain the persistence of epithelial microinvasion by these mutants. Importantly, while epithelial microinvasion, cellular reorganization, the innate epithelial immune response, and the propensity to cause invasive disease following pneumococcal colonisation are all strain-dependent, no single determinant explained these differences.

The complexity of the interaction between *S. pneumoniae* and the mucosal epithelium was highlighted using a primary epithelial cell infection model (29). This model, consisting of Clara cells (involved in secretory, xenobiotic metabolic, and progenitor cell functions), goblet cells (mucus production), ciliated cells (responsible for mucus and small particle transport), exhibited considerable epithelial cellular re-organisation involving β catenin, acetylated tubulin and uteroglobin. In a rabbit pneumococcal meningitis model, increased acetylated tubulin and microtubule stabilisation was attributed to pneumolysin activity (16). Previously, using a pneumolysin deficient mutant of *S. pneumoniae* serotype 4 (TIGR4), we have shown that pneumolysin is a key driver of the epithelial inflammatory response to pneumococcal infection (3). Based on these findings, we propose that differential expression of pneumolysin, and H_2O_2 by the WT and mutant strains may contribute to the distinct patterns of epithelial reorganisation and responses that we observed. These have the potential to influence both bacterial clearance and transmission (1).

Epithelial infection with the 6B WT and Δ*proABC/piaA* strains induced innate inflammatory pathway gene expression typical of pneumococcal infection (3), including cytokine/chemokines, interleukins, Toll Like Receptor and NFκB signalling, alongside apoptotic transcripts such as FOXO3 and TP53. Notably, some epithelial genes were upregulated exclusively during WT infection, which could be related to its greater disease-causing potential. These are involved in RNA degradation, O-linked

glycosylation, wnt signalling, DNA sensing, RIG-I pathways all of which play a role in the immune response and signal transduction. In contrast, the Δ*fhs/piaA* strain activated a distinct pro-survival and adaptation profile, upregulating genes such as JUN, SMARCA4, NFAT5, KLF6 and TCF4, which are involved in homeostatic signalling and chromatin remodelling (30, 31). This suggests of a more tolerant epithelial response to the Δ*fhs/piaA* strain. Ultimately, these capsule-independent differences in pneumococcal-epithelial interactions may shape the adaptive immune response to pneumococcal colonisation (14, 32), which could then further influence colonisation dynamics and disease progression. However, the extent to which these responses impact the duration of nasopharyngeal carriage, invasiveness, transmission, or clearance remains to be determined.

Importantly, while all strains adhered and microinvade the epithelium, WT serotype 6B infection led to pneumococcal transmigration, a more pro-inflammatory innate immune transcriptomic profile and increased caspase 8 activity, indicative of a robust cellular response to *S. pneumoniae*, the Δ*proABC/piaA* and Δ*fhs/piaA* strains exhibited attenuation in many of these characteristics. However, epithelial cell reorganisation (expression of acetylated tubulin, uteroglobin and β catenin) were more readily affected following infection with the Δ*proABC/piaA* and Δ*fhs/piaA* strains compared to WT, which may partially explain differences observed in epithelial transcriptomic responses observed. This suggests that pneumococcal sensing by the epithelium is driven by capsule-independent factors (12, 34).

The *proABC* operon consists of three genes involved in proline biosynthesis (ProABC)(35). *fhs* catalyses the synthesis of N10 formyl tetrahydrofolate, essential for carbon metabolism and purine nucleotide biosynthesis in various bacterial species (36, 37), particularly under hypoxic conditions (37, 38). Increasing evidence suggests that bacterial virulence and metabolism are intricately linked (39). Whether the distinct epithelial innate immune response to Δ*fhs/piaA* infection is due to diminished NFκB and MAPK activation (potentially linked to extracellular receptor engagement),

reduced caspase 8 activity mediated by enhanced pneumococcal H_2O_2 release, decreased pneumolysin activity, or a compensatory metabolic response to the stress remains to be determined.

S. pneumoniae is highly adapted to colonise the human host and transmit from person to person. Invasive pneumococcal disease, particularly in its most severe forms, represents an evolutionary dead end. Our findings suggest that epithelial innate immune activation is not necessarily linked to disease potential. As seen in 'professional' intracellular bacterial species such as *Listeria* and *Salmonella*, the host response to microinvasion might also promote pneumococcal transmission (40, 41). Whether the less pro-inflammatory Δ*fhs/piaA* is less transmissible than the more inflammatory WT is unknown, but this could be explored further using the EHPC model (42).

In conclusion, these data further support our proposed paradigm that epithelial microinvasion by *S. pneumoniae* in healthy people is frequent and does not necessarily lead to disease. Microinvasion may however aid transmission through immune evasion and localised inflammation and transmigration across the epithelium may represent the first step towards transition to invasive disease. Our findings also highlight the broad-ranging effects of single gene mutations in pneumococcal biosynthesis pathways, which may explain the complexity of differences between seemingly closely related strains. The interplay between *S. pneumoniae* and the host epithelium is modulated by key mediators such as hydrogen peroxide and pneumolysin, which can have both enhancing and inhibitory effects on epithelial immune responses depending on the infection context. However, strain differences in subsequent epithelial cell microinvasion, cellular reorganisation and inflammatory responses appear to be driven by the differential expression of multiple bacterial virulence and metabolic pathways, rather than any single determinant.

METHODS AND PROTOCOLS

Bacteria

The *Streptococcus pneumoniae* serotype 6B (strain BHN 418(46)) was a kind gift from Prof. Birgitta Henriques Normark (Karolinska Institute). Δ*proABC/piaA* and Δ*fhs/piaA* mutant strains were generated using overlap extension PCR as described by Ramos-Sevillano *et al*(28). Stocks of bacteria were stored at -80ºC when bacterial growth in Todd Hewitt Broth (THY) was 0.3 $O.D._{600nm}$. Aliquots were defrosted, centrifuged at 8000g for eight minutes and resuspended in 1% Fetal Bovine Serum (FBS, Gibco) in MEM media (Gibco) for infections. Approximately 10 bacteria were added for every epithelial cell. Colony forming units (CFU) were counted by serial dilutions on horse blood agar plates (EO Labs). Starting inoculums were not significantly different across strains for all assays.

Bacterial RNA-seq sample collection, sequencing and reads

Mutant pneumococcal strains (three biological replicates for each mutant) and 6B WT (three biological replicates) were grown in THY to mid log phase and the pellets resuspended in THY and undiluted human serum for 60mins. The culture was then pelleted, and RNA stored in RNA Protect at -70ºC before extracting total RNA (47). Total RNA from each library was ribo-depleted and sent for Illumina Next Seq Sequencing Pathogen Genomics Unit (PGU), UCL. The quality of raw FASTQ reads was checked by FastQC v0.11.5, Babraham Bioinformatics, UK (48) and visualised using multiQC v1.9 (49). Reads were trimmed using Trimmomatic 0.39 (50). Trimmed reads were also checked by FastQC and multiQC. Trimmed reads were then mapped to KEGG annotated 6B genome sequence (670-6B, Accession: CP002176.1) using bowtie2 with default settings(51). Conversion into BAM files was performed using SAMtools (52). Mapped reads were visualized in the Integrated Genome Browser (IGB) (53). FeatureCounts v2.0.0 was used to summarize read counts for each annotated feature in the respective reference genomes in multimapping mode (-M) (54).

Differential gene expression analyses

The generated count matrix was imported into R-studio (R v3.4.2) and normalization of counts and differential gene expression analysis was performed by DESeq2 (55). DESeq2 normalized libraries

were regularized log transformed for visualizing heatmaps and clustering. Differential gene expression was performed on raw counts. Fold change shrinkage was implemented with the apeglm package within DESeq2. Genes with a log2 fold change > 1.5 and false discovery rate (FDR) of < 0.05 were categorized as differentially expressed. KEGG pathway enrichment and module analysis were performed on differentially regulated genes using over representation analysis (ORA) implemented by clusterProfiler (56).

Experimental Human Pneumococcal Carriage Model (EHPC)

A full explanation of experimental design and selection criteria has been previously described (3). Following written informed consent, healthy non-smoking adults between the ages of 18 – 59 were inoculated with 80,000 CFU/nostril live strains of *S. pneumoniae*. Mucosal cells from the inferior turbinate using a plastic Rhino-probe™ (curettage, Arlington Scientific) were collected prior to inoculation, and days 2 and 6 post-inoculation. Samples were processed for confocal microscopy analysis. Nasal wash samples were collected for CFU count analysis. There were no adverse events. Ethical approval was given by NHS Research and Ethics Committee (REC)/Liverpool School of Tropical Medicine (LSTM) REC, reference number: 18/NW/0481 and Human Tissue Authority licensing number 12548.

Normal Human Epithelial Cells

Normal Human Bronchial/Tracheal Epithelial Cells (NHBE-A, ATCC® PCS-300-010™) were plated at $6x10^3$ cells/cm^2 on a layer of sub-lethally γ-irradiated (60 Gy) mouse embryonic fibroblasts 3T3-J2 cells (kind donation from Howard Green, Harvard Medical School, Boston(57)) with keratinocyte culture medium cFAD (3:1 DMEM (Gibco) to Ham F-12 Nut Mix (Gibco), 10% FBS (HyClone, Sigma), 1% Penicillin-Streptomycin (100X, Sigma), 0.4 µg/mL Hydrocortisone (Calbiochem, USA), 5 µg/ml Insulin (various), 10-10 Cholera Toxin (Sigma) and 2x10-9 Triodothyronine (Sigma)). Epithelial cells were stimulated with 10 ng/mL human epidermal growth factor (hEGF, PeproTech, USA) on days 3 and 5. Cultures were grown at 37°C 6% CO_2 and sub-confluent cultures were trypsinised with 0.25%

Trypsin-EDTA (Sigma). For NHBE-A differentiation in Air Liquid Interface (ALI) culture, cells were plated at a density of $6x10^4/cm^2$ on 1µm pore PET cell culture inserts (12 wells, Greiner). The insert was supplemented with cFAD medium on the top and bottom. After 48 hours, medium was removed from the top of the culture (exposure) and the culture was fed with fresh PneumaCult™ differentiation Medium (Stemcell Technologies) from the bottom of the well every 2 days for 3 weeks, until cell ciliation was observed. Antibiotics were removed from the medium and cells washed 24 hours before infection experiments.

Human Epithelial Cell Lines

Human pharyngeal carcinoma Detroit 562 epithelial cells (ATCC_CCL-138) were grown in 10% FCS in alpha MEM media (Gibco). For each set of experiments, cells were used within 5 passages. Cells consistently tested PCR negative for mycoplasma (Cambridge Biosciences).

Pneumococcal-epithelial cell co-culture

For association and internalisation assays, confluent monolayers of Detroit 562 cells (typically day 7 - 8 post plating) cultured on 12 well plates (Corning), were exposed to *S. pneumoniae* (Multiplicity of infection: 1 cell to 10 pneumococci) for three hours in 1% FCS alpha MEM (six-hour infection for HNBE-A cells in 1% Pneumocult media without supplements) (3). Cells washed three times in $HBSS^{+/+}$ before incubation in 1% saponin for 10 minutes at 37°C to lyse cells. Bacterial dilutions were plated on horse blood agar for 16 hours and colony forming units counted. For internalisation quantification, 200µg/ml gentamicin was added to the cells for one hour before incubation with saponin.

For transmigration assays, Detroit 562 cells were plated onto 3µm pore, PET Transwell Inserts (ThermoFisher) typically for 10 days (3). Media was changed to 1% FCS (250µl apical chamber, 1ml basal chamber) one hour prior to infection experiments. 1mg/ml FITC-dextran (Sigma Aldrich) was added to the apical chamber of selected inserts for permeability assays. Transepithelial Electrical Resistance (TEER) was measured before and after infection using an EVOM2 (World Precision

Instruments). Bacteria were added to the cells for three hours during of which 50µl of basal media was repeatedly removed to measure bacterial load by counting CFU/well. Permeability was recorded using a FLUOstar Omega (BMG Labtech) at 488nm.

Confocal Microscopy

Sample processing was performed as previously described(3). Briefly, mucosal cells from the EHPC model were placed directly into 4% PFA and cytospun onto microscope slides. NHBE-A cells and Detroit 562 cells cultured on transwell membranes were fixed in 4% PFA (Pierce, Methanol Free). Cells were permeabilised with 0.2% Triton X-100 for 10 minutes, blocked for one hour in blocking buffer (3% goat serum and 3% BSA in PBS (Sigma)) and incubated with pneumococcal antisera Pool Q (raised against the polysaccharide capsule, SSI Diagnostica) for one hour. Wheat germ agglutinin conjugated to Rhodamine (Vector Labs) was added along with goat-anti rabbit IgG conjugated to Alexa Fluor 488 for 45 minutes in blocking buffer. Primary (used at 1:100) antibodies used for epithelial cell proteins can be found in Supplemental Information Table 2. Secondary (used at 1:500) antibodies were either goat anti-mouse or goat anti-rabbit – Alexa Fluor 555 or 546, ThermoFisher. Of note, for epithelial protein antibodies raised in rabbit (Uteroglobin), no pneumococcal staining was possible and therefore pneumococci were not visible on the images. DAPI was added for 5 minutes and cells were mounted with Aqua PolyMount (VWR International) and a coverslip on the microslide. Pneumococci were recorded by manual scanning of the whole cytospin for the EHPC samples. More than three fields of view were recorded for each bacterial strain for Detroit 562 cell infections, using inverted Zeiss LSM (either 700 or 880) confocal microscopes. Images were processed with Zeiss LSM Image Browser. Z stacks were recorded at 1µm intervals at either 40x oil or 63x oil objectives. Automated image analysis was carried out using Cellprofiler (58).

Electron Microscopy

Preparation of Detroit 562 cells and NHBE-A cells was identical and previously described (3). Briefly, cells cultured on transwells were fixed with 2% paraformaldehyde and 1.5% glutaraldehyde in 0.1 M

cacodylate buffer and post-fixed in 1% OsO4 / 1.5% K4Fe(CN)6 in 0.1 M cacodylate buffer pH7.3. For scanning electron microscopy, samples were dehydrated in graded ethanol-water series and infiltrated with Agar 100 resin mix. Ultra-thin sections were cut at 70-80 nm using a diamond knife on a Reichert ultracut microtome. Sections were collected on 300 mesh copper grids and stained with lead citrate. For transmission electron microscopy the samples were hardened at 60°C for 48 hours. The coverslip was removed, and a representative area was selected. Ultra-thin sections were cut at 70-80 nm using a diamond knife on a Reichert ultra-cut S microtome. Sections were collected on copper grids and stained with lead citrate. Samples were viewed with a Joel 1010 transition electron microscope and the images recorded using a Gatan Orius CCD camera.

Pneumolysin activity

Adapted from Kirkham et al(59). Briefly, final concentration of 2% horse blood (EO Labs) solution was prepared in phenol free alpha MEM (Life Technologies) and 100 µl added to wells of a 96 U-bottom plate (Corning). 100 µl of bacterial solutions (containing ~2.5×10^6 bacteria) were suspended in phenol free alpha MEM were added to each 96 well. Saponin was used as a positive control for lysis. Solutions were incubated for 30 minutes at 37°C before centrifugation at 1000g for one minute. 100 µl was transferred into a new 96 well plate and absorbance recorded at 540nm on a plate reader.

Hydrogen Peroxide Assay

Detroit 562 cells were cultured in white 96 well plates (Corning). NHBE-A cells were cultured in 12 well plates in Pneumocult media. Cells were incubated with H_2O_2 substrate and infected with strains of *S. pneumoniae* for up to six hours according to manufacturers' instructions (ROS-Glo™ H_2O_2 Assay, Promega). ROS-Glo™ Detection solution was added to the cells and incubated for 20 minutes. For primary cells, supernatant was then transferred to a white 96 well plate. Luminescence was read using a GloMax -Multi Detection System plate reader (Promega).

Caspase assay

Detroit 562 cells were cultured in white 96 well plates (Corning). NHBE-A cells were cultured in 12 well plates in Pneumocult media. Cells were infected with strains of *S. pneumoniae* for up to six hours. Primary cell supernatant was transferred to a white 96 well plate. Samples were incubated with Caspase-Glo® 1 Reagent, Caspase-Glo® 1 YVAD-CHO Reagent, Caspase-Glo® Z-VAD-FMK Reagent or Caspase-Glo® 8 Reagent, for one hour and according to manufacturers' instructions (Promega). Luminescence was read using a GloMax-Multi Detection System plate reader (Promega).

RNA samples and sequencing (RNA-Seq)

RNA-Seq data was collected as previously described (3). Confluent monolayers of Detroit 562 epithelial cells were infected with S. pneumoniae strains for four hours before collection in RNALater. RNA was extracted using a Qiagen RNAEasy micro kit and treated for DNA removal using a Qiagen Turbo DNA-free kit. RNA quality was assessed and quantified using a BioAnalyser (Agilent 2100). Samples were sequenced using Illumina Nextseq 500/550 High Output 75 cycle kit giving 15-20 million 41bp paired-end reads per sample (Pathogens Genomic Unit, UCL).

Statistics

Each condition within each experiment was performed in duplicate or triplicate, and each experiment was performed independently more than three times, unless stated otherwise. Error bars represent SEM, unless stated otherwise. GraphPad Prism Version 7 was used for parametric (t-tests or ANOVA) or non-parametric (Mann-Whitney or Kruskal-Wallis tests) analysis, which was based on the Shapiro-Wilk normality test. Ad hoc tests were performed using Tukey's (for parametric data) or Dunn's (for non-parametric data) multiple comparisons test. P values less than 0.05 were considered significant.

Data and code availability

Source data are provided as a Source Data file. RNAseq data from the Detroit 562 cell infections is publicly accessible through Zenodo with Accession (DOI:10.5281/zenodo.7997789).

ACKNOWLEDGEMENTS

This study was funded by CMW from a Postdoctoral Innovation Award from UCL, a Pump-Priming Award and Enhancement Award from the Human Infection Challenge Network for Vaccine Development (HIC-VAC (funded by the GCRF Networks in Vaccines Research and Development) which is co-funded by the MRC and BBSRC). This UK funded award is part of the EDCTP2 programme supported by the European Union. CMW and RSH are supported by the Medical Research Council (grant MR/T016329/1). The authors would like to thank Prof. Peter Hermans (Radboud University Medical Centre) for donating the 6B pneumococcal strain originally from Prof. Birgitta Henriques-Normark (Karolinska Institute) and obtained directly from DF at LSTM. EHPC sample collection was supported by the Medical Research Council (grant MR/M011569/1), Bill and Melinda Gates Foundation (grant OPP1117728) awarded to DF and the National Institute for Health Research (NIHR) Local Comprehensive Research Network. The authors also wish to thank the EHPC Clinical Team at LSTM and all the volunteers. Confocal imaging facilities at LSTM were funded by a Wellcome Trust Multi-User Equipment Grant (104936/Z/14/Z). Electron microscopy processing and image capture was performed by Dr. Elizabeth Slavik-Smith in the Biosciences EM facility at UCL. MC is supported by a Springboard to Independence grant (AirwayStasis) from the French Government's Investissement d'Avenir program, the Laboratoire d'Excellence "Integrative Biology of Emerging Infectious Diseases" (ANR-10-LABX-62-IBEID) and the Chromatin and infection unit headed by Melanie A. Hamon. RNA-Seq library preparation was undertaken at UCL through the UCL/UCLH Biomedical Research Centre and MRC funded Pathogen Genomics Unit (PGU, G0900950). All RNAseq data processing was completed by the PGU. MN is supported by the Wellcome Trust and by NIHR Biomedical Research Centre Funding to University College Hospitals NHS Foundation Trust and University College London. RR is supported by Marie Skłodowska-Curie Individual Fellowships 896014. PB is supported by the European Research Council (ERC-Stg No. 639429), the Rosetrees Trust (M362-F1; M553), the CF Trust (SRC006;SRC020), the London

Advanced Therapies - Research England (C2N-AT.006), the MRC Confidence in Concept scheme (Award: MC_PC_17180), the Innovate UK (Smart grant n.10005465), the Duchenne Parent Project (DPP) and the NIHR GOSH BRC. MW is supported by a 223065 Wellcome Investigator Award to Clare Jolly, UCL. ERS and JSB are supported by MRC grant R/N02687X/1 and Wellcome grant 221803/Z/20/Z. JSB, MN, and RSH acknowledge funding from the Department of Health's National Institute of Health and Care Research Biomedical Research Centre funding to UCL and UCLH. RSH is a NIHR Senior Investigator.

AUTHOR CONTRIBUTIONS: CMW conceived, funded, designed and conducted the study, performed the experiments, acquired samples and processed data, and wrote the first draft of the manuscript. GP analysed and interpreted the RNAseq data. MB analysed and interpreted the bacterial transcriptomic data. RR cultured and differentiated primary epithelial cells. ERS generated the 6B mutant strains and bacterial transcriptomic data. JR collected and processed EHPC samples. JAGA processed the RNA-Seq data. MW ran the image analysis. MC provided technical advice. PB and CJ provided investigator support. MN provided RNA-Seq analysis support. DF provided investigator support and EHPC clinical samples. JSB generated the 6B mutant strains, interpreted the data and revised the manuscript. RSH provided investigator support, designed and interpreted the data, revised the manuscript. All authors commented on and approved the manuscript.

COMPETING INTERESTS: The authors declare no competing interests.

REFERENCES

1. Weiser JN, Ferreira DM, Paton JC. Streptococcus pneumoniae: transmission, colonization and invasion. Nat Rev Microbiol. 2018;16(6):355-67.
2. O'Brien KL, Wolfson LJ, Watt JP, Henkle E, Deloria-Knoll M, McCall N, et al. Burden of disease caused by Streptococcus pneumoniae in children younger than 5 years: global estimates. Lancet. 2009;374(9693):893-902.
3. Weight CM, Venturini C, Pojar S, Jochems SP, Reine J, Nikolaou E, et al. Microinvasion by Streptococcus pneumoniae induces epithelial innate immunity during colonisation at the human mucosal surface. Nat Commun. 2019;10(1):3060.

634 4. Zafar MA, Hamaguchi S, Zangari T, Cammer M, Weiser JN. Capsule Type and Amount Affect Shedding
635 and Transmission of Streptococcus pneumoniae. mBio. 2017;8(4).
636 5. Amin-Chowdhury Z, Collins S, Sheppard C, Litt D, Fry NK, Andrews N, Ladhani SN. Characteristics of
637 Invasive Pneumococcal Disease Caused by Emerging Serotypes After the Introduction of the 13-Valent
638 Pneumococcal Conjugate Vaccine in England: A Prospective Observational Cohort Study, 2014-2018. Clin
639 Infect Dis. 2020;71(8):e235-e43.
640 6. Echlin H, Frank M, Rock C, Rosch JW. Role of the pyruvate metabolic network on carbohydrate
641 metabolism and virulence in Streptococcus pneumoniae. Mol Microbiol. 2020;114(4):536-52.
642 7. Hartel T, Eylert E, Schulz C, Petruschka L, Gierok P, Grubmuller S, et al. Characterization of central
643 carbon metabolism of Streptococcus pneumoniae by isotopologue profiling. J Biol Chem. 2012;287(6):4260-
644 74.
645 8. Henriques-Normark B, Tuomanen EI. The pneumococcus: epidemiology, microbiology, and
646 pathogenesis. Cold Spring Harb Perspect Med. 2013;3(7).
647 9. Kohler S, Voss F, Gomez Mejia A, Brown JS, Hammerschmidt S. Pneumococcal lipoproteins involved
648 in bacterial fitness, virulence, and immune evasion. FEBS Lett. 2016;590(21):3820-39.
649 10. van Opijnen T, Camilli A. A fine scale phenotype-genotype virulence map of a bacterial pathogen.
650 Genome Res. 2012;22(12):2541-51.
651 11. Subramanian K, Neill DR, Malak HA, Spelmink L, Khandaker S, Dalla Libera Marchiori G, et al.
652 Pneumolysin binds to the mannose receptor C type 1 (MRC-1) leading to anti-inflammatory responses and
653 enhanced pneumococcal survival. Nat Microbiol. 2019;4(1):62-70.
654 12. Periselneris J, Turner CT, Ercoli G, Szylar G, Weight CM, Thurston T, et al. Pneumolysin suppresses
655 the initial macrophage pro-inflammatory response to Streptococcus pneumoniae. Immunology.
656 2022;167(3):413-27.
657 13. Gladstone RA, Lo SW, Lees JA, Croucher NJ, van Tonder AJ, Corander J, et al. International genomic
658 definition of pneumococcal lineages, to contextualise disease, antibiotic resistance and vaccine impact.
659 EBioMedicine. 2019;43:338-46.
660 14. Ferreira DM, Neill DR, Bangert M, Gritzfeld JF, Green N, Wright AK, et al. Controlled human infection
661 and rechallenge with Streptococcus pneumoniae reveals the protective efficacy of carriage in healthy adults.
662 Am J Respir Crit Care Med. 2013;187(8):855-64.
663 15. Eshun-Wilson L, Zhang R, Portran D, Nachury MV, Toso DB, Lohr T, et al. Effects of alpha-tubulin
664 acetylation on microtubule structure and stability. Proc Natl Acad Sci U S A. 2019;116(21):10366-71.
665 16. Iliev AI, Djannatian JR, Opazo F, Gerber J, Nau R, Mitchell TJ, Wouters FS. Rapid microtubule bundling
666 and stabilization by the Streptococcus pneumoniae neurotoxin pneumolysin in a cholesterol-dependent,
667 non-lytic and Src-kinase dependent manner inhibits intracellular trafficking. Mol Microbiol. 2009;71(2):461-
668 77.
669 17. Surabhi S, Jachmann LH, Shumba P, Burchhardt G, Hammerschmidt S, Siemens N. Hydrogen Peroxide
670 Is Crucial for NLRP3 Inflammasome-Mediated IL-1beta Production and Cell Death in Pneumococcal Infections
671 of Bronchial Epithelial Cells. J Innate Immun. 2022;14(3):192-206.
672 18. Maekawa T, Kashkar H, Coll NS. Dying in self-defence: a comparative overview of immunogenic cell
673 death signalling in animals and plants. Cell Death Differ. 2023;30(2):258-68.
674 19. Gunther C, Buchen B, He GW, Hornef M, Torow N, Neumann H, et al. Caspase-8 controls the gut
675 response to microbial challenges by Tnf-alpha-dependent and independent pathways. Gut. 2015;64(4):601-
676 10.
677 20. Gonzalez-Juarbe N, Bradley KM, Shenoy AT, Gilley RP, Reyes LF, Hinojosa CA, et al. Pore-forming
678 toxin-mediated ion dysregulation leads to death receptor-independent necroptosis of lung epithelial cells
679 during bacterial pneumonia. Cell Death Differ. 2017;24(5):917-28.
680 21. Gonzalez-Juarbe N, Bradley KM, Riegler AN, Reyes LF, Brissac T, Park SS, et al. Bacterial Pore-Forming
681 Toxins Promote the Activation of Caspases in Parallel to Necroptosis to Enhance Alarmin Release and
682 Inflammation During Pneumonia. Sci Rep. 2018;8(1):5846.
683 22. Erttmann SF, Gekara NO. Hydrogen peroxide release by bacteria suppresses inflammasome-
684 dependent innate immunity. Nat Commun. 2019;10(1):3493.

685 23. Alibayov B, Scasny A, Khan F, Creel A, Smith P, Vidal AGJ, et al. Oxidative Reactions Catalyzed by
686 Hydrogen Peroxide Produced by Streptococcus pneumoniae and Other Streptococci Cause the Release and
687 Degradation of Heme from Hemoglobin. Infect Immun. 2022;90(12):e0047122.
688 24. Zafar MA, Wang Y, Hamaguchi S, Weiser JN. Host-to-Host Transmission of Streptococcus pneumoniae
689 Is Driven by Its Inflammatory Toxin, Pneumolysin. Cell Host Microbe. 2017;21(1):73-83.
690 25. Terra VS, Plumptre CD, Wall EC, Brown JS, Wren BW. Construction of a pneumolysin deficient mutant
691 in streptococcus pneumoniae serotype 1 strain 519/43 and phenotypic characterisation. Microb Pathog.
692 2020;141:103999.
693 26. Bazant J, Ott B, Hudel M, Hain T, Lucas R, Mraheil MA. Impact of Endogenous Pneumococcal
694 Hydrogen Peroxide on the Activity and Release of Pneumolysin. Toxins (Basel). 2023;15(10).
695 27. Ramos-Sevillano E, Ercoli G, Betts M, Guerra-Assuncao JA, Iverson A, Frank M, et al. Essential role of
696 proline synthesis and the one-carbon metabolism pathways for systemic virulence of Streptococcus
697 pneumoniae. mBio. 2024;15(11):e0175824.
698 28. Ramos-Sevillano E, Ercoli G, Felgner P, Ramiro de Assis R, Nakajima R, Goldblatt D, et al. Preclinical
699 Development of Virulence Attenuated Streptococcus pneumoniae Strains Able to Enhance Protective
700 Immunity Against Pneumococcal Infection. Am J Respir Crit Care Med. 2020.
701 29. Travaglini KJ, Nabhan AN, Penland L, Sinha R, Gillich A, Sit RV, et al. A molecular cell atlas of the
702 human lung from single-cell RNA sequencing. Nature. 2020;587(7835):619-25.
703 30. Herta T, Bhattacharyya A, Bollensdorf C, Kabus C, Garcia P, Suttorp N, et al. DNA-release by
704 Streptococcus pneumoniae autolysin LytA induced Krueppel-like factor 4 expression in macrophages. Sci Rep.
705 2018;8(1):5723.
706 31. Barutcu AR, Lajoie BR, Fritz AJ, McCord RP, Nickerson JA, van Wijnen AJ, et al. SMARCA4 regulates
707 gene expression and higher-order chromatin structure in proliferating mammary epithelial cells. Genome
708 Res. 2016;26(9):1188-201.
709 32. Wilson R, Cohen JM, Jose RJ, de Vogel C, Baxendale H, Brown JS. Protection against Streptococcus
710 pneumoniae lung infection after nasopharyngeal colonization requires both humoral and cellular immune
711 responses. Mucosal Immunol. 2015;8(3):627-39.
712 33. Hill H ME, Nikolaou E, Blizard A, Pojar S, Howard A, Hyder-Wright A, Devin J, Reiné J, Robinson R,
713 Solórzano C, Jochems S, Kenny-Nyazika T, Ramos-Sevillano E, Weight CM, Myerscough C, McLennan D,
714 MortonB , Gibbons E, Farrar M, Randles V, Burhan H, Chen T, Shandling AD, Campo JJ, Heyderman RS, Gordon
715 SB, Brown JS, Collins AM, Ferreira DM. A Randomised Controlled Trial of Nasal Immunisation with Live
716 Virulence Attenuated Streptococcus pneumoniae Strains using Human Infection Challenge. Medrxiv. 2023.
717 34. Periselneris J, Ercoli G, Pollard T, Chimalapati S, Camberlein E, Szylar G, et al. Relative Contributions
718 of Extracellular and Internalized Bacteria to Early Macrophage Proinflammatory Responses to Streptococcus
719 pneumoniae. mBio. 2019;10(5).
720 35. Belitsky BR, Brill J, Bremer E, Sonenshein AL. Multiple genes for the last step of proline biosynthesis
721 in Bacillus subtilis. J Bacteriol. 2001;183(14):4389-92.
722 36. Crowley PJ, Gutierrez JA, Hillman JD, Bleiweis AS. Genetic and physiologic analysis of a formyl-
723 tetrahydrofolate synthetase mutant of Streptococcus mutans. J Bacteriol. 1997;179(5):1563-72.
724 37. Sah S, Aluri S, Rex K, Varshney U. One-carbon metabolic pathway rewiring in Escherichia coli reveals
725 an evolutionary advantage of 10-formyltetrahydrofolate synthetase (Fhs) in survival under hypoxia. J
726 Bacteriol. 2015;197(4):717-26.
727 38. Aluri S, Rex K, Varshney U. Simultaneous presence of fhs and purT genes is disadvantageous for the
728 fitness of Escherichia coli growth. FEMS Microbiol Lett. 2015;362(14).
729 39. Obolski U, Swarthout TD, Kalizang'oma A, Mwalukomo TS, Chan JM, Weight CM, et al. The metabolic,
730 virulence and antimicrobial resistance profiles of colonising Streptococcus pneumoniae shift after PCV13
731 introduction in urban Malawi. Nat Commun. 2023;14(1):7477.
732 40. Galan JE. Salmonella Typhimurium and inflammation: a pathogen-centric affair. Nat Rev Microbiol.
733 2021;19(11):716-25.
734 41. Li G, Wang G, Li M, Li L, Liu H, Sun M, Wen Z. Morin inhibits Listeria monocytogenes virulence in vivo
735 and in vitro by targeting listeriolysin O and inflammation. BMC Microbiol. 2020;20(1):112.
736 42. Connor V, German E, Pojar S, Mitsi E, Hales C, Nikolaou E, et al. Hands are vehicles for transmission
737 of Streptococcus pneumoniae in novel controlled human infection study. Eur Respir J. 2018;52(4).

43. Lourenco J, Daon Y, Gori A, Obolski U. Pneumococcal Competition Modulates Antibiotic Resistance in the Pre-Vaccination Era: A Modelling Study. Vaccines (Basel). 2021;9(3).
44. Watkins ER, Kalizang'Oma A, Gori A, Gupta S, Heyderman RS. Factors affecting antimicrobial resistance in Streptococcus pneumoniae following vaccination introduction. Trends Microbiol. 2022;30(12):1135-45.
45. Chaguza C, Senghore M, Bojang E, Gladstone RA, Lo SW, Tientcheu PE, et al. Within-host microevolution of Streptococcus pneumoniae is rapid and adaptive during natural colonisation. Nat Commun. 2020;11(1):3442.
46. Browall S, Norman M, Tangrot J, Galanis I, Sjostrom K, Dagerhamn J, et al. Intraclonal variations among Streptococcus pneumoniae isolates influence the likelihood of invasive disease in children. J Infect Dis. 2014;209(3):377-88.
47. Ramos-Sevillano E. EG, Guerra-Assunção J.F., Betts M., Partridge F., Fernandes V.E., Wall E., Gordon S.B., Ferreira D.M., Heyderman R.S., Brown J.S. Essential role of proline synthesis and the one-carbon metabolism pathways for systemic virulence of Streptococcus pneumoniae. Biorxiv. 2023.
48. S. A. FastQC: a quality control tool for high throughput sequence data. 2010.
49. Ewels P, Magnusson M, Lundin S, Kaller M. MultiQC: summarize analysis results for multiple tools and samples in a single report. Bioinformatics. 2016;32(19):3047-8.
50. Bolger AM, Lohse M, Usadel B. Trimmomatic: a flexible trimmer for Illumina sequence data. Bioinformatics. 2014;30(15):2114-20.
51. Langmead B, Salzberg SL. Fast gapped-read alignment with Bowtie 2. Nat Methods. 2012;9(4):357-9.
52. Li H, Handsaker B, Wysoker A, Fennell T, Ruan J, Homer N, et al. The Sequence Alignment/Map format and SAMtools. Bioinformatics. 2009;25(16):2078-9.
53. Nicol JW, Helt GA, Blanchard SG, Jr., Raja A, Loraine AE. The Integrated Genome Browser: free software for distribution and exploration of genome-scale datasets. Bioinformatics. 2009;25(20):2730-1.
54. Liao Y, Smyth GK, Shi W. featureCounts: an efficient general purpose program for assigning sequence reads to genomic features. Bioinformatics. 2014;30(7):923-30.
55. Love MI, Huber W, Anders S. Moderated estimation of fold change and dispersion for RNA-seq data with DESeq2. Genome Biol. 2014;15(12):550.
56. Yu G, Wang LG, Han Y, He QY. clusterProfiler: an R package for comparing biological themes among gene clusters. OMICS. 2012;16(5):284-7.
57. Rheinwald JG, Green H. Serial cultivation of strains of human epidermal keratinocytes: the formation of keratinizing colonies from single cells. Cell. 1975;6(3):331-43.
58. Carpenter AE, Jones TR, Lamprecht MR, Clarke C, Kang IH, Friman O, et al. CellProfiler: image analysis software for identifying and quantifying cell phenotypes. Genome Biol. 2006;7(10):R100.
59. Kirkham LA, Kerr AR, Douce GR, Paterson GK, Dilts DA, Liu DF, Mitchell TJ. Construction and immunological characterization of a novel nontoxic protective pneumolysin mutant for use in future pneumococcal vaccines. Infect Immun. 2006;74(1):586-93.

FIGURE LEGENDS

Fig 1. Pneumococcal – epithelial interactions in the EHPC model. (A) Schematic showing that during colonisation, pneumococci adhere to the epithelial cell surface (association), internalise inside epithelial cells (microinvasion). Mucus – lime; pneumococci – purple; intracellular vacuole – dark

green; epithelial cells – yellow; nucleus – brown; cell junctions – pink. (B) Representative microscopy images showing pneumococcal-epithelial interactions by the 6B WT, Δ*proABC/piaA* or Δ*fhs/piaA* mutants. Surface carbohydrates (red), nuclei (DAPI, blue), pneumococci (green). (C) Table summarising the microscopy and microbiology counts for each inoculated strain 6 days post challenge per volunteer. Adherent represents pneumococcal surface association and intracellular represents pneumococci that have microinvaded (inside) epithelial cells.

Fig 2. Impact of pneumococcal infection on NHBE-A cell junctional protein expression and barrier integrity. NHBE-A Cells were cultured at ALI and infected with pneumococcal strains for 6hrs. (A) Top: Representative confocal microscopy images from 4 independent experiments with replicates, showing pneumococcal (green) association with the epithelium (red, surface carbohydrates; nuclei blue) at 6hr post infection. Bottom: Representative transmission electron microscopy images from 2 independent experiments, showing pneumococcal microinvasion examples of each strain (arrows), enclosed within a vacuole after 4hr infection. Representative confocal microscopy images from four independent experiments with replicates showing pneumococcal (green) interactions with junctional proteins (red); JAM-A (B), ZO-1 (C) and β catenin (D) in primary HBE-A cells after a 6hr exposure. Nuclei stained with DAPI in blue. Co-localisation of junctional proteins and pneumococci appear yellow, as highlighted by arrows. (E) Integrated intensity of β catenin in pneumococcal negative (not pneumococcal associated) or positive (pneumococcal associated) cells. Non infected v pneumococcal negative cells **** p <0.0001 (NI v Δ*proABC/piaA*), ** p = 0.0026 (NI v Δ*fhs/piaA*); non-infected v pneumococcal positive cells; **** p <0.0001 (NI v Δ*proABC/piaA* and NI v Δ*fhs/piaA*); Kruskal-Wallis, n = 4 independent experiments. (F) Transepithelial electrical resistance (TEER) was recorded pre- and post- 6hr infection to assess barrier integrity. N = 3 independent experiments with replicates. Average TEER pre-infection was 466Ω.cm^2 (430-484 Ω.cm^2, p = 0.1458 ANOVA) and average TEER post-infection was 545Ω.cm^2 (527-567 Ω.cm^2. p = 0.04744 ANOVA). Change in TEER comparing non-infected cells to infected cells p = 0.6592, Kruskal-Wallis. Error bars represent SEM.

Fig 3. Pneumococcal – epithelial interactions with NHBE-A**.** Cells were cultured at ALI and infected with pneumococcal strains for 6hrs. (A) Representative scanning electron microscopy images from 2 independent experiments, showing the surface of the epithelium. Representative examples of differentiated epithelia (basal cells, Clara cells, goblet cells, ciliated cells) are shown in yellow text. Colonising pneumococci are highlighted by arrows. Representative confocal microscopy images from 4 independent experiments with replicates for (B) Ciliated cells (acetylated tubulin, red), (C) Goblet cells (mucin5ac, red, (arrows indicate co-localisation of mucin5ac with pneumococci)), (D) Clara cells (uteroglobin, red) after 6hr infection. Pneumococci (green), nuclei (DAPI, blue), colocalization of red and green appears as yellow. Integrated intensity of Muc5ac (E) or acetylated tubulin (F) in pneumococcal negative or positive cells from two or more images. Mucin5ac, neg p = 0.6852, pos p = 0.8510, Acetylated tubulin, neg p = 0.2677, pos p = 0.017, ANOVA. N = 3 or 4 independent experiments. (G) Integrated intensity of uteroglobin normalised to non-infected cells (left, p = 0.0115 non-infected v infected, Kruskal-Wallis) and percentage of Clara positive cells following infection (right, p = 0.0003 non-infected v strains, p = 0.0036 6B v mutant strains, Kruskal-Wallis). N = 3 independent experiments.

Fig 4. **Strain association, microinvasion and transmigration of Detroit 562 cells.** Cells were infected with *S. pneumoniae* for three hours and CFU counts recorded. (A) Representative confocal microscopy images from 6 independent experiments with replicates, showing pneumococcal (green) interactions with surface carbohydrates (red). (B) Association of pneumococcal strains to epithelial cells. p = 0.0009 (Kruskal-Wallis), n = 6 with replicates. (C) Internalisation of strains into cells, following a gentamicin protection assay. p = 0.0219 (Kruskal-Wallis) N = 6 with replicates. (D) Pneumococcal viability inside epithelial cells following a gentamicin protection assay. n = 3 or 4 independent experiments with replicates. Counts were normalised to microinvasion counts for each strain after 3 hours infection and compared to 6B WT; +1hr p = 0.6517, +2hr p = 0.1377, +3hr p = 0.1183 (ANOVA). (E) Transmigration of pneumococcal strains across confluent monolayers on transwell inserts. CFUs were recorded from the basal chamber. N = 6 independent experiments with replicates. p < 0.001 (Kruskal-Wallis). (F) Representative confocal microscopy images from 6

independent experiments with replicates, showing pneumococcal (green) interactions with β catenin (red). Nuclear DAPI stain (blue).

Fig 5. Detroit 562 cell transcriptomic responses to pneumococcal strains. Epithelial cells were infected for four hours with pneumococcal strains and RNA extracted and processed for RNAseq. 6B n = 11, PP n = 17, FP n = 14, non-infected n = 12, from 6 independent experiments. (A) All significantly log2 fold change upregulated genes according to strain compared to non-infected cells. Significance was defined as DEGs with a log2 fold change (logFC) of > 1.5 and false discovery rate (FDR) of < 0.05. (B) Comparison of the top 20 most upregulated genes for each strain, compared to non-infected cells. Upstream regulator analysis for (C) transcription factors and (D) kinases.

Fig 6. Effects of pneumococcal infection on caspase activity in Detroit 562 cells. Caspase activity was assessed by luminescence, following infection with pneumococcal strains for 6 hours. (A) Caspase 3/7 activity was determined following incubation with the specific inhibitor Z-VAD-FMK. N = 4 with replicates. In comparison to non-infected cells, caspase 3/7 $p = 0.0022$; caspase 3/7 + Z-VAD-FMK inhibitor $p = 0.0005$. In comparison to 6B WT, caspase 3/7 $p = 0.0215$; caspase 3/7 + Z-VAD-FMK inhibitor $p = 0.0012$ (Kruskal-Wallis). (B) Caspase 1 activity was determined following incubation with the specific inhibitor YVAD-CHO. Negative signals indicate caspase activity other than caspase 1. N = 6 with replicates. In comparison to non-infected cells, $p = 0.39$; caspase+YVAD-CHO inhibitor $p = 0.3604$ and, in comparison to 6B WT, $p = 0.6226$; caspase+YVAD-CHO inhibitor $p = 0.5386$ (Kruskal-Wallis). (C) Caspase 8 activity was assessed following infection with pneumococcal strains. N = 3 with replicates. In comparison to non-infected cells, $p = 0.0015$ (ANOVA) and, in comparison to 6B WT, $p = 0.0172$ (ANOVA).

Fig 7. Hydrogen peroxide secretion and pneumolysin activity from pneumococcal strains in the absence and presence of Detroit 562 cells. (A) Fold change of hydrogen peroxide production from the mutants compared to WT, normalised to the CFU counts. 3hr $p = 0.0087$ (ANOVA), 6hr p

= 0.0209 (Kruskal-Wallis). (B) Fold change of hydrogen peroxide production from the mutants compared to WT, normalised to the CFU counts, following infection of Detroit 562 cells. Media was replaced after 1hr infection and cells incubated for a further 5hrs. N = 3 independent experiments with replicates. Compared to 6B WT, p = 0.0034 (ANOVA). (C) Pneumolysin activity was assessed using a red blood cell lysis assay. Strains were incubated with red blood cells for 30 minutes and absorbance measured. N = 4 experiments with replicates. Pneumococcal strain haemolytic activity is calculated in comparison to 100% lysis by 0.0625% saponin. p <0.0001 compared to 6B WT (ANOVA).

Figure 1. Pneumococcal – epithelial interactions in the EHPC model

A

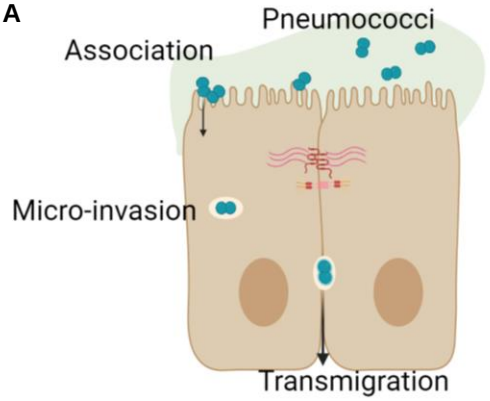

B

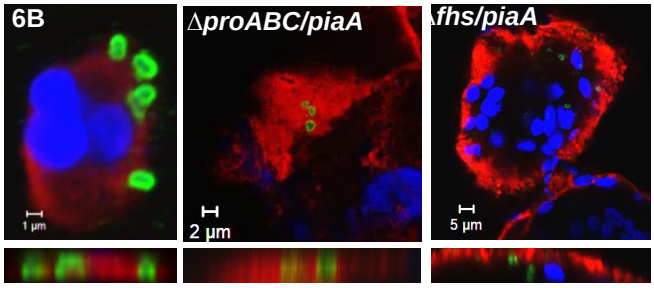

C

6B	MICROSCOPY		MICROBIOLOGY
	Adherent	Intracellular	
#1	0	0	0
#2	2	0	520
#3	0	0	0
#4	1	0	0
#5	0	0	9
#6	1	2	223
#7	0	0	5725
#8	39	4	1110
#9	0	0	0
#10	0	0	767
#11	0	0	0

Δ*proABC/piaA*	MICROSCOPY		MICROBIOLOGY
	Adherent	Intracellular	
#1	0	0	0
#2	0	0	0
#3	0	0	0
#4	5	3	0
#5	3	2	0
#6	8	2	5
#7	0	0	0
#8	0	2	0
#9	0	2	1
#10	0	0	0
#11	0	0	0

Δ*fhs/piaA*	MICROSCOPY		MICROBIOLOGY
	Adherent	Intracellular	
#1	2	0	21856
#2	1	3	0
#3	3	3	16
#4	51	54	0
#5	0	0	520325

Figure 2. Impact of pneumococcal infection on NHBE-A cell junctional protein expression and barrier integrity.

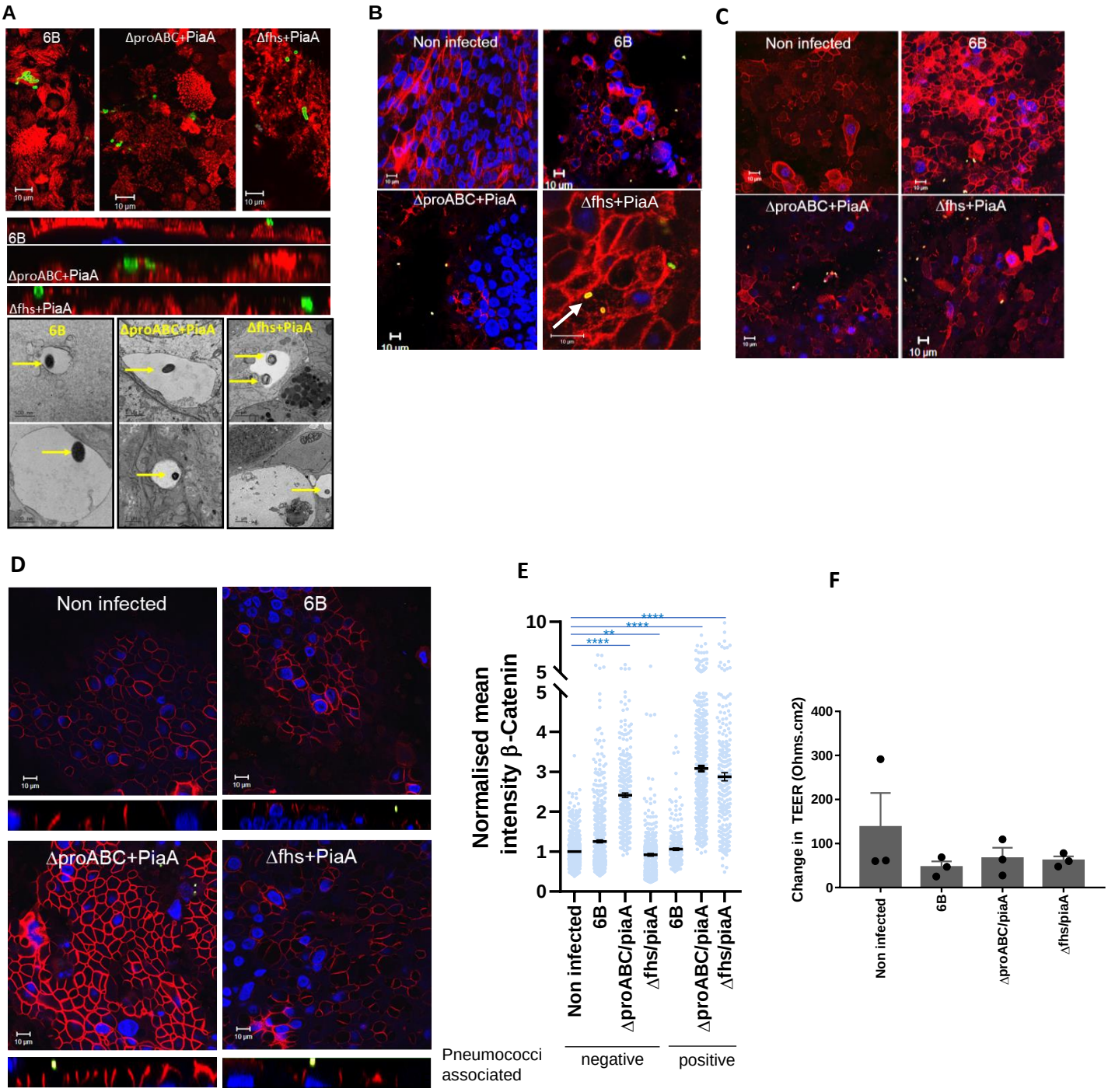

Figure 3. Pneumococcal – epithelial interactions with primary human epithelial cells.

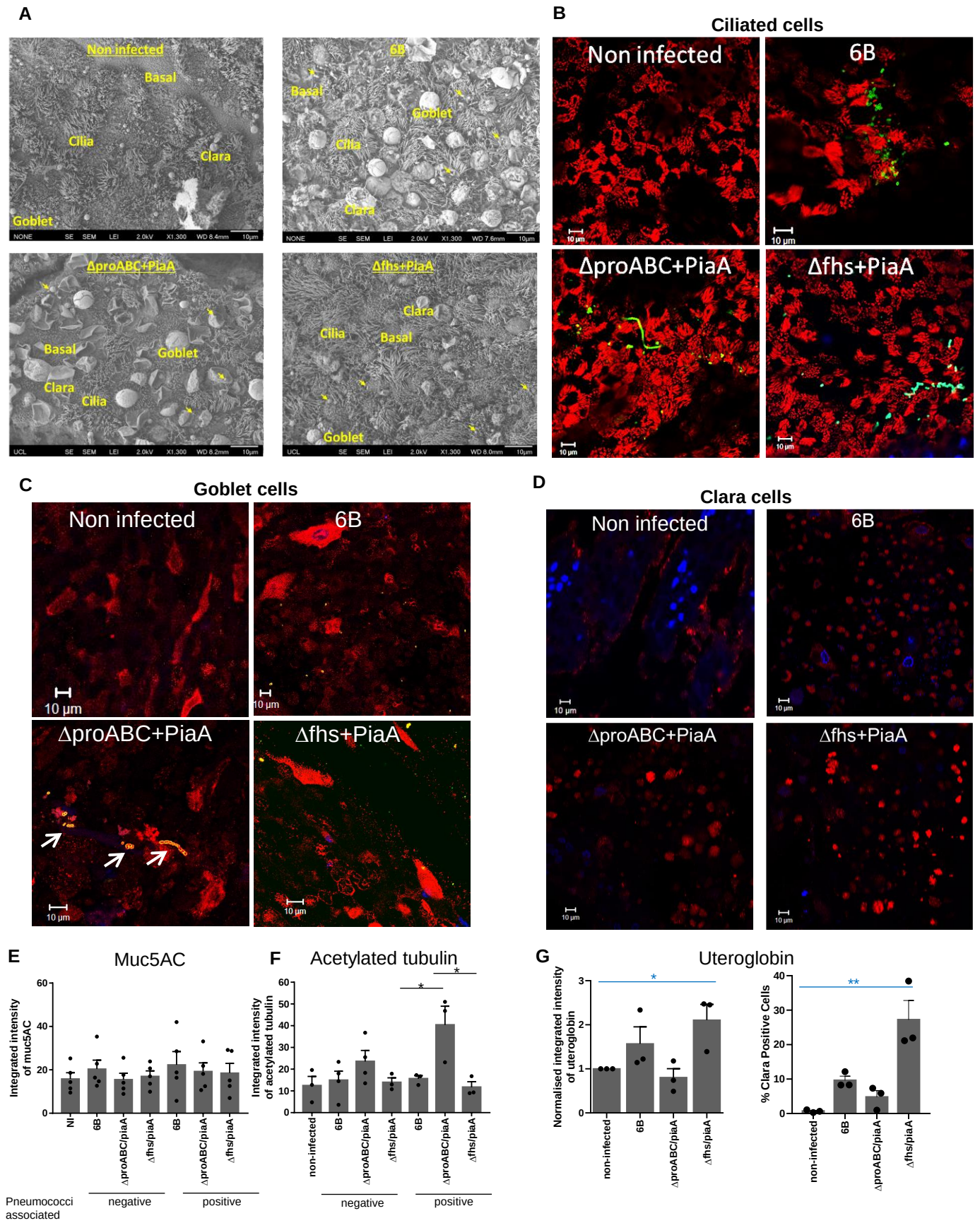

Figure 4. Strain association, microinvasion and transmigration of Detroit 562 cells.

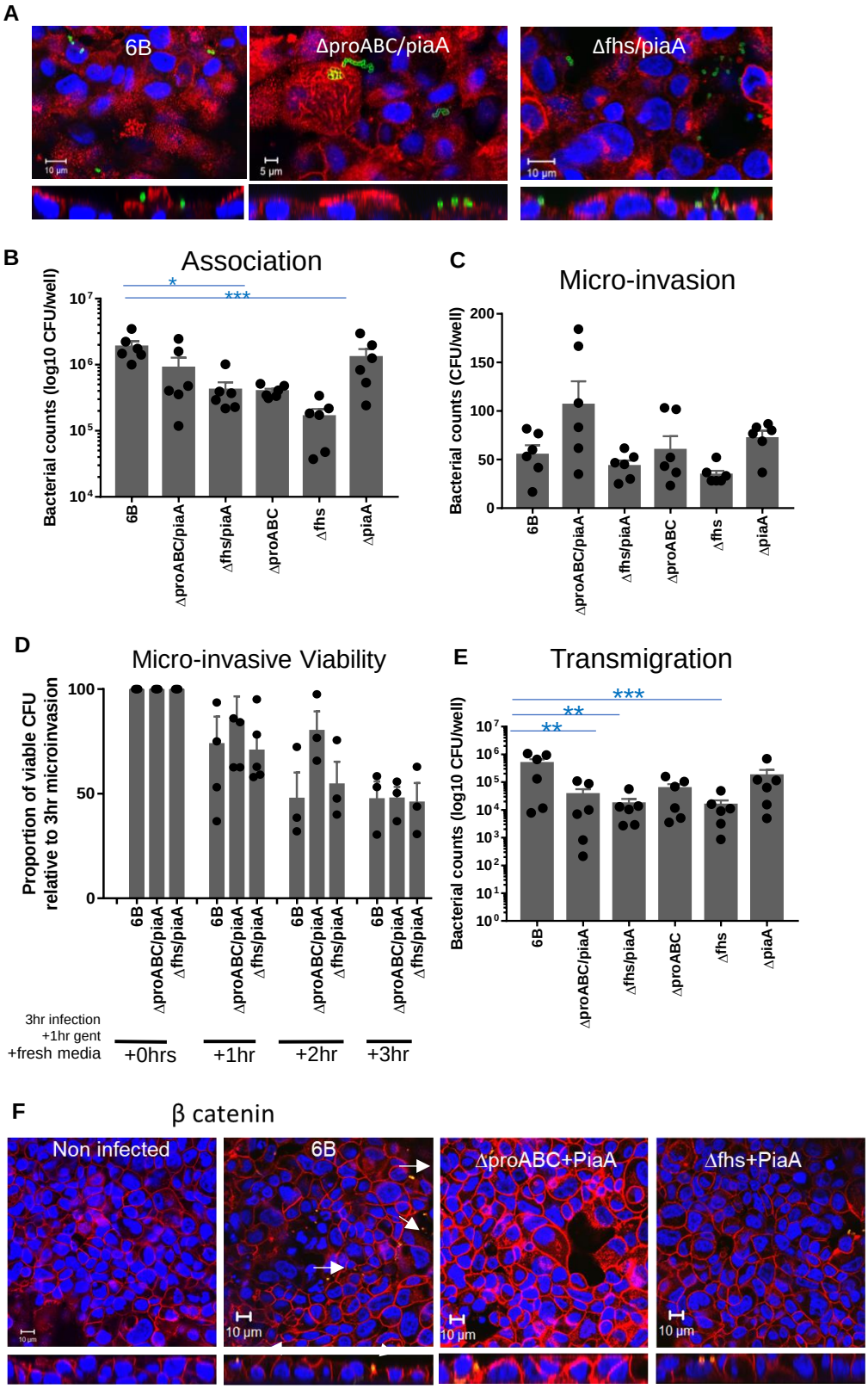

Figure 5. Detroit 562 cell transcriptomic responses to pneumococcal strains.

A

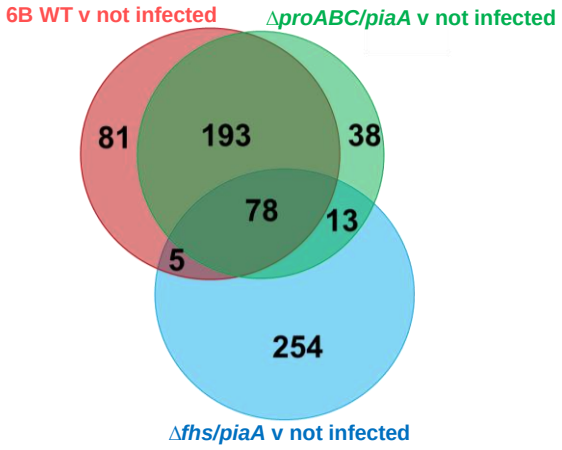

B

log2foldchange	6B	ΔproABC/piaA	Δfhs/piaA
Upregulated genes			
AC256236.1	32.9	25.5	0.0
AC022149.1	30.2	27.6	0.0
Z84488.2	29.1	21.6	0.0
MUC21	25.8	29.0	0.0
VASN	20.9	0.0	0.0
BRD2	18.4	24.7	0.0
AC012254.2	18.2	13.8	0.0
CTAGE4	18.1	0.0	0.0
MICE	17.1	20.3	0.0
AC107075.1	10.1	0.0	0.0
CSNK2B	0.0	20.2	0.0
MTRNR2L6	0.0	19.4	15.8
LSM2	0.0	17.1	0.0
ALOX5	0.0	0.0	6.9
AC006064.6	0.0	0.0	3.4
TAP2	0.0	0.0	3.2
CYP1A1	0.0	0.0	1.7
FOSB	0.0	0.0	1.4
IL1B	0.0	0.0	1.3
CXCL8	0.0	0.0	1.1
CXCL2	0.0	0.0	1.1
CYP1B1	0.0	0.0	1.0

C

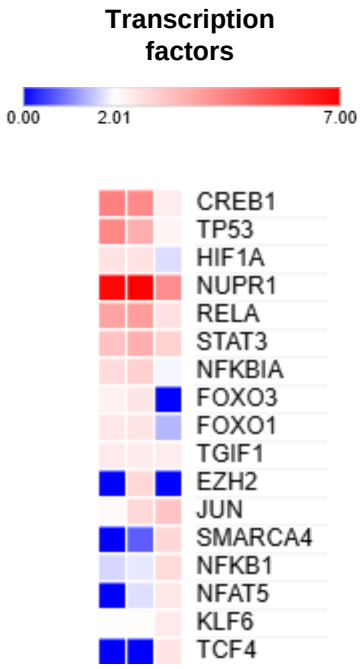

D

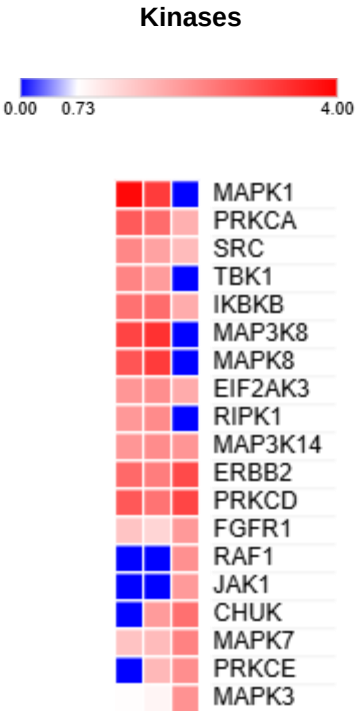

Figure 6. Effects of pneumococcal infection on caspase activity in Detroit 562 cells.

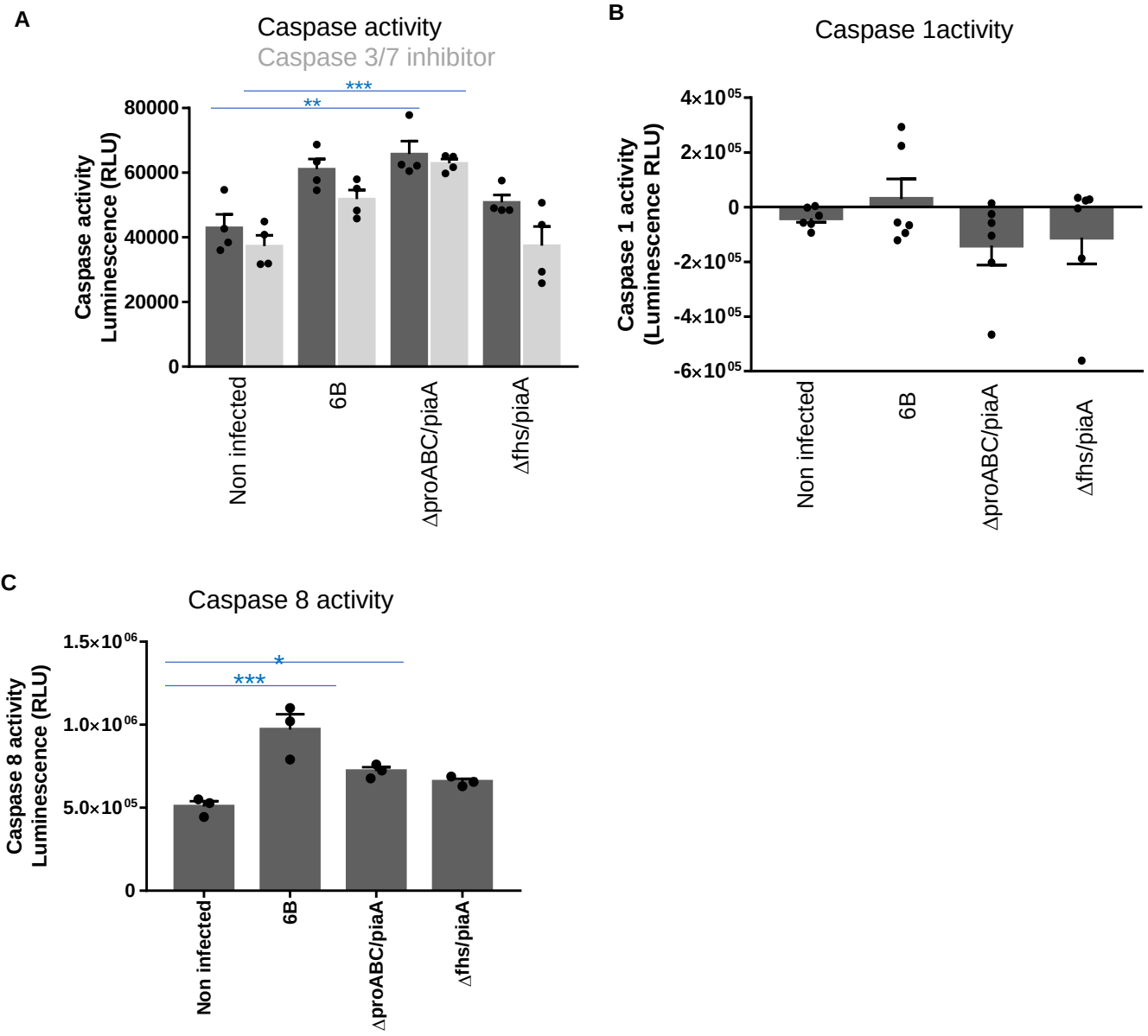

Figure 7. Hydrogen peroxide secretion and pneumolysin activity from pneumococcal strains in the absence and presence of Detroit 562 cells.

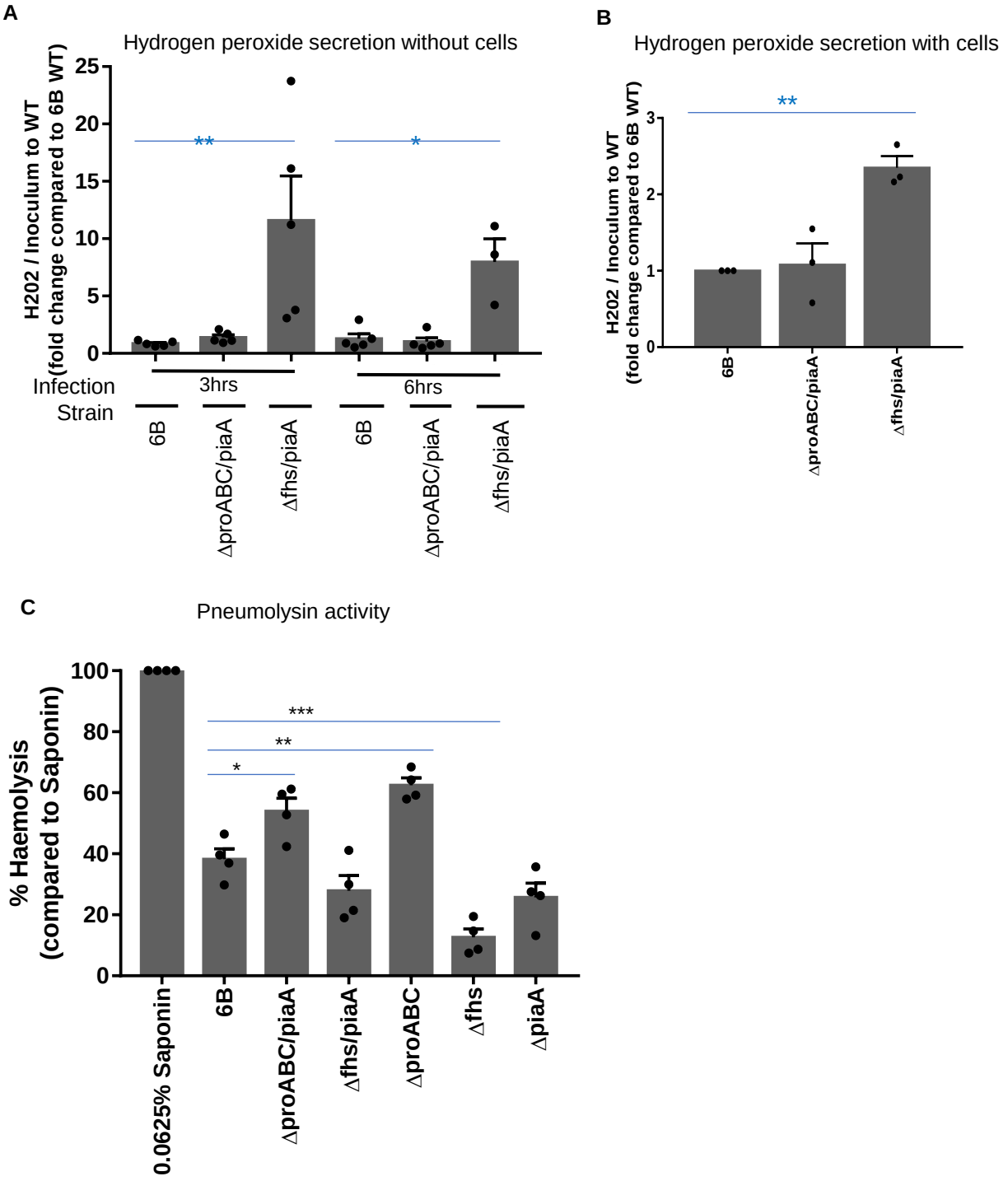
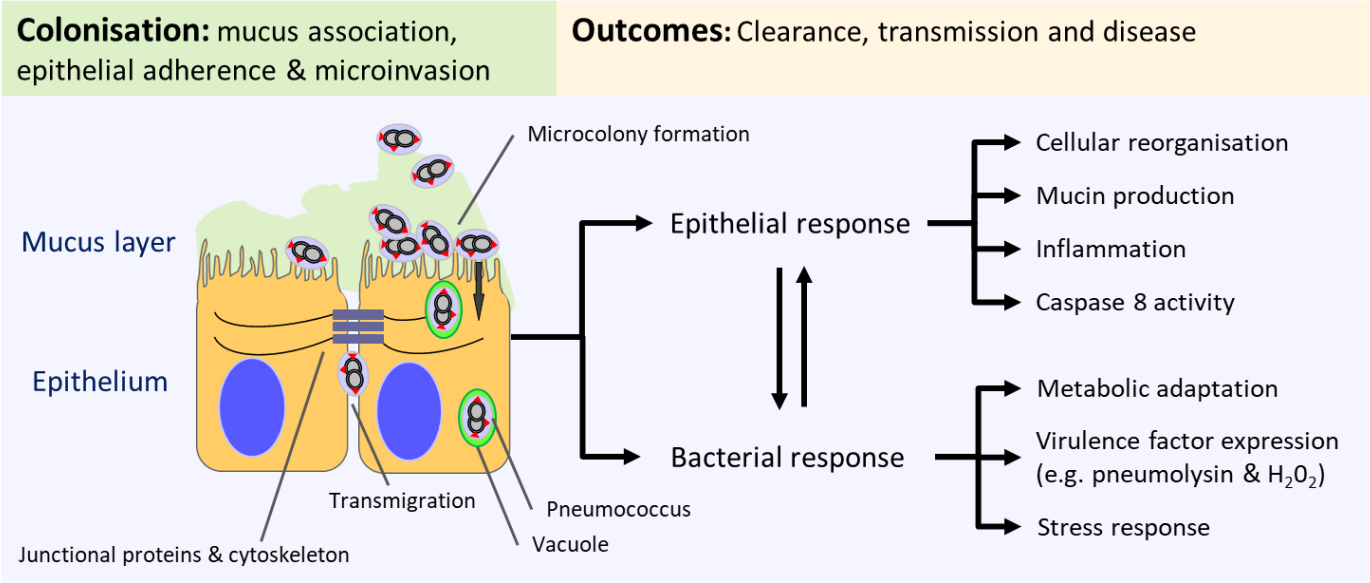
Graphical abstract